Optimizing the Structural and Photocatalytic Properties of TiO_2 Composites Synthesized via Sol-Gel Method

Vipul B. Shinde[1], Karankumar R. Sature[1], S. J. Indurkar[1], Y. K. Lahamate[1], Nilkanth N. Kapse[2], Kumar Rajesh Singh[1], Vishal A. Pandit[1], K. G. Joshi[3], Shivnarayan B. Bajaj[1*]

[1]*Department of Physics, J. E. S., R. G. Bagdia Arts, S. B. Lakhotia Comerce and R. Bezonji Science College, Jalna, MS, India*
[2]*Department of Physics, B. Raghunath ACS College, Parbhani – 431 401, (MS) India.*
[3]*Assistant Professor, CES Department, Sanjivani University, Ahmednagar, India*
Email: vipulshinde22@gmail.com

Abstract: Titanium dioxide (TiO_2) is widely studied for its photocatalytic and optical properties, but its performance can be enhanced by forming composites with other materials. This research focuses on synthesizing TiO_2 composites using the sol-gel technique by incorporating Al_2O_3, WO_3, ZnO, CNT, and SiNT. Additionally, optimizing the calcination process by modifying time and temperature is crucial to improving structural and functional characteristics. TiO_2 composites were synthesized via the sol-gel method, followed by controlled calcination under varying temperature and time conditions. X-ray diffraction (XRD) was employed to analyze the crystalline phases, while surface area and porosity were examined to assess material properties. UV-Visible spectroscopy was used to study the absorption spectra and band structure alterations in the composites. XRD analysis confirmed that the TiO_2-Al_2O_3 composite contained both anatase and rutile phases, along with Al_2O_3, exhibiting a specific surface area of 32.1 m^2/g and an average crystallite size of 18.09 nm. The TiO_2-WO_3 composite demonstrated the formation of a mixed oxide system at the interface, altering its electronic properties. Optical absorption spectra revealed significant modifications in band structures, affecting light absorption and photocatalytic efficiency. The structural and optical characteristics of TiO_2 composites were significantly influenced by the choice of secondary material and calcination conditions. The findings suggest that optimizing these parameters can enhance photocatalytic performance, making TiO_2 composites promising for applications in environmental remediation and materials science.

Keywords: TiO_2 composites, sol-gel synthesis, photocatalysis, X-ray diffraction, calcination, optical properties, band structure, nanomaterials.

1. Introduction

TiO_2 has a long history of application. However, it was not economically viable until the early twentieth century [1]. Kronos, a German chemical firm, developed large-scale TiO_2 production in the 1920s [2]. TiO_2 may be generated using synthetic rutile, a chemical derivative of ilmenite, or naturally occurring ilmenite [3-7].

TiO_2 exists in three forms: rutile, anatase, and leucoxene. Rutile is a common kind recognized for its high refractive index and remarkable stability. While anatase and leucoxene are uncommon, they offer unique properties that may be useful in specific circumstances [8]. TiO_2 is a common pigment for paints, coatings, polymers, and paper owing to its good scattering properties and refractive index. It also improves the brightness, hardness, and acid resistance of porcelain enamels when employed as an opacifier and whitening agent [9, 10]. TiO_2's strong heat resistance makes it widely employed in industrial applications. These uses include missiles, power plants, airplanes, armor plate, and naval vessels [11-14].

Recent research suggests that TiO_2 has strong photocatalytic activity. Research shows that TiO_2 is a very efficient photocatalyst for removing organic pollutants. This is owing to its cheap cost, high chemical stability, and ecologically friendly properties [15-18]. TiO_2 has unique qualities that have led scientists to create solutions for air and water filtration, as well as self-cleaning surfaces. TiO_2 is becoming more popular for renewable energy applications. Recent research has explored the possible advantages of TiO_2 in energy conversion technologies, such as improving solar cell efficiency [19-21].
Researchers encounter several problems while creating TiO_2 composites. These challenges include regulating particle shape and size, ensuring stability, and attaining uniform dispersion. Researchers are now studying creative techniques to overcome these restrictions. Researchers are looking at novel synthesis procedures, adjusting current ones, and using additives to increase stability and dispersion. Furthermore, researchers apply modern characterisation tools to get a deeper understanding of the composite material's properties [22].
There are many ways for generating TiO_2 compounds, including solid-state reaction, coprecipitation, chemical vapor deposition, hydrothermal approach, sol-gel method, and electrochemical deposition [3, 18]. Various variables influence the experimental method for synthesizing TiO_2 compounds. These criteria include the components used, the compound's desirable qualities, and the intended use. The sol-gel process may create TiO_2 composites with unique properties for many applications [23-26].
This study aims to employ the sol-gel process to make TiO_2 composites with Al_2O_3, WO_3, ZnO, CNT, and SiNT. The purpose is to optimize the calcination parameters by adjusting the temperature and time. A comprehensive investigation will be conducted to evaluate the structural and optical properties of the composites that have been manufactured, as well as to determine their surface area and porosity. By improving TiO_2 composites durability and effectiveness, the researchers want to make them more useful for a range of applications.

2. Methodology

2.1 Synthesis of TiO_2 using the sol-gel
Isopropyl alcohol (IPA) and titanium tetra isopropoxide (TTIP) swirled together to form a continuous sol-gel solution (SGS). Nitric acid (HNO_3) and distilled water was combined drop by drop to create a homogenous solution. At 80^0 C, the liquid was then agitated until it took on the consistency of gel and solidified into a little lump. The TiO_2 gel was heated to 550° C and calcined for six hours in a furnace. The sample underwent a particular calcination process before cooling to room temperature for further examination to examine its structural and optical properties. This dependable experimental method uses the sol-gel procedure to produce TiO_2.
2.2 Synthesis of TiO_2 Composites.
The sol-gel method yielded nano crystalline TiO_2 molecules. The updated method comprises dispersing 0.3 g of the nano crystalline material in 40 ml of isopropyl alcohol and gradually adding titanium isopropoxide (TTIP) to the mixture. TTIP is a predecessor of TiO_2. Following that, the mixture was carefully stirred until it reached a uniform texture. To establish uniformity, Al_2O_3, WO_3, ZnO, CNT, and SiNT were mixed in comparable proportions with TiO_2. The mixture was stirred again. At room temperature, the solution solidified for 24 hours. Following the gelation method, the gel was dried at 100°C for 12 hours to ensure that all solvent had been removed. Extensive study shows that heating the dried gel at 550°C for six hours yields the greatest TiO_2 production results. The composite was ready for use after the calcination step and subsequent cooling to room temperature. This novel approach manufactures TiO_2 composites with suitable nanocrystalline material utilizing a sol-gel process.
2.3 Characterization Techniques
X-ray diffraction (XRD) was used to analyze the phase composition and crystal structure of the TiO_2 nanocomposite. We used a Cu-Kα radiation diffractometer to get XRD patterns. The samples were scanned at a constant rate of one degree per minute throughout a 2θ range of 10 to 70 degrees. We investigated the optical properties of the TiO_2 nanocomposite using UV-vis spectroscopy. This approach allows for the assessment of the sample's light absorption and transmission at various wavelengths. BET measurements assessed the surface area and pore size distribution of the TiO_2 nanocomposite. BET analysis may be used to assess the surface area and pore size distribution by measuring the quantity of gas (often nitrogen) adsorbed onto the sample's surface at different pressure levels.

3. Result and Discussion

3.1. X-Ray Analysis

The mixed anatase-rutile nanocrystalline TiO_2 nanoparticles were analysed structurally using the XRD technique. X-ray diffractometer measurements using a BROOKER D8 employed Cu Kα irradiation (λ = 0.154 nm). The diffraction spectra of the (101) anatase and (110) rutile peaks were obtained with a step width of 0.1 degrees during survey scans ranging from 20° to 80°.

3.2 X-Ray Analysis for TiO_2 Composites

This work explored the X-ray diffraction patterns of TiO_2 composites consisting of SiNT, CNT, WO_3, Al_2O_3, and ZnO. The ideal temperature and time were found to be 550 °C and 6 hours, respectively. The composites' X-ray diffraction patterns were measured and evaluated. Figure 3 shows the X-ray diffraction pattern of the TiO_2-Al_2O_3 composite, revealing the existence of the Al_2O_3 phase alongside TiO_2's anatase and rutile phases. Figure 4 depicts the XRD patterns of the remaining composites, as seen in Figure 7. The composite materials of ZnO, CNT, and SiNT include both anatase and rutile phases of TiO_2. The research found that the sol-gel technique is successful for producing TiO_2 composites from diverse materials. The calcination parameters have a considerable influence on the crystallite morphologies and phases of the final composite.

3.2.1 TiO_2–Al_2O_3 Composite

The TiO_2-Al_2O_3 composite consists of TiO_2 anatase, rutile, and Al_2O_3 phases.The composite contains a higher concentration of anatase TiO_2 compared to the pure TiO_2 sample. Al_2O_3 functions as a nucleating agent, enhancing the presence of the anatase phase in composites. According to the XRD pattern, the composite contains Al_2O_3, as indicated by a peak at 37.6°. At an angle of 65.9°, there is evidence of a combination of aluminum and titanium oxides. This indicates the possibility of a solid solution or composite between titanium dioxide (TiO_2) and aluminum oxide (Al_2O_3). Al_2O_3 has formed on the surface of TiO_2 in the mixed oxide system. Al_2O_3 exhibits higher surface energy compared to TiO_2, resulting in accelerated surface growth.

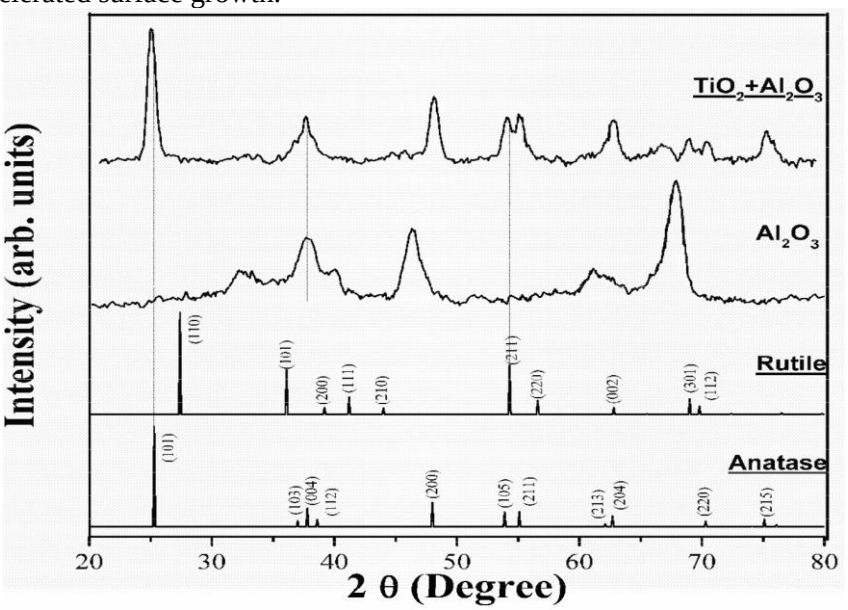

Figure 1. XRD pattern of an Al_2O_3 and TiO_2 composite.

Our study using the Scherrer formula reveals that the TiO_2 crystallite size in the composite material corresponds to 18.1 nm. These crystals have a somewhat lower size than pure TiO_2, suggesting that Al_2O_3 inclusion in the compound could stop TiO_2 crystal development. X-ray diffraction investigations reveal that the TiO_2- Al_2O_3 composite has a unique crystal structure that distinguishes it from both pure TiO_2 and pure Al_2O_3.

3.2.2 Composite TiO_2-WO_3

Figure 2 shows the X-ray diffraction (XRD) pattern of the TiO_2-WO_3 composite, thereby exposing the main component as the anatase phase of TiO_2. Moreover, the composite has quite high concentrations of rutile phase of TiO_2. The composite exhibits a maximum intensity of anatase TiO_2, greater than that of the pure TiO_2 sample, suggesting that WO_3 facilitates the development of the anatase phase. Obviously, the highest peak in the anatase phase points in the (101) plane for anatase TiO_2. The XRD

pattern shows a clear peak at 54.3° suggesting the likely presence of the WO_3 phase in the composite material. The observations suggest that W and Ti are present in a mixed oxide environment. The maximum noted at 62.66° points to the location of this system near the border between WO_3 and TiO_2. This suggests the surface of TiO_2 has developed WO_3. An essential system in the field as this composite has the ability to greatly increase its photocatalytic activity.

Our investigation utilizing the Scherrer formula and looking at the full width at half-maximum (FWHM) of the diffraction peak indicates that the TiO_2 crystallite has a size of 15.26 nm | By providing a larger surface area for reactions, the small dimensions of the TiO_2 crystallites in the composite have benefits in photocatalytic uses. The WO_3 phase shows as larger particles or aggregates with a crystallite size of 27.1 nm, higher than that of TiO_2.

Generally, in this study the TiO_2-WO_3 composite analysis demonstrates the presence of both W and Ti at the two phase contact. WO_3 addition into the system raises the anatase phase production of TiO_2. Improved photocatalytic activity of the composite may be explained in part by WO_3 inclusion and TiO_2 crystal small size.

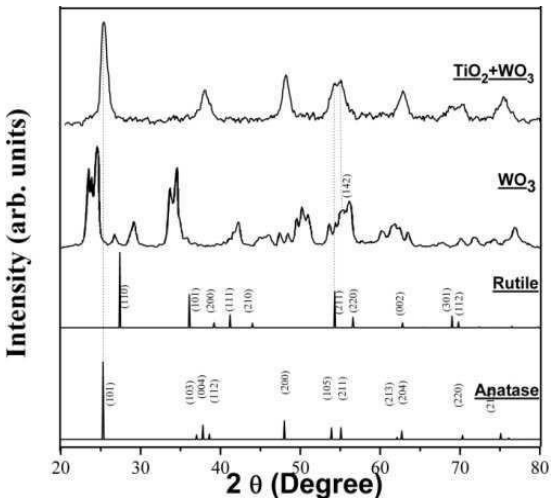

Figure 2. XRD pattern of TiO2 and WO_3 composite.

3.2.3 Composite TiO_2-ZnO

Figure 3 shows the XRD pattern of a Zn-containing TiO_2 composite, indicating the existence of the anatase and rutile phases of TiO_2. Compared to pure TiO_2 samples, this sample shows a higher concentration of the rutile phase. One may deduce that the rutile phase has developed in the TiO_2 based on the intensity of the peak in the (110) planes. The composite contains ZnO, as evidenced by the peak at 36.3°. Based on the observed peaks at various angles, it appears that the sample contains a mixed oxide system, which likely includes Zn and Ti. These peaks indicate that ZnO is forming on the surface of TiO_2.

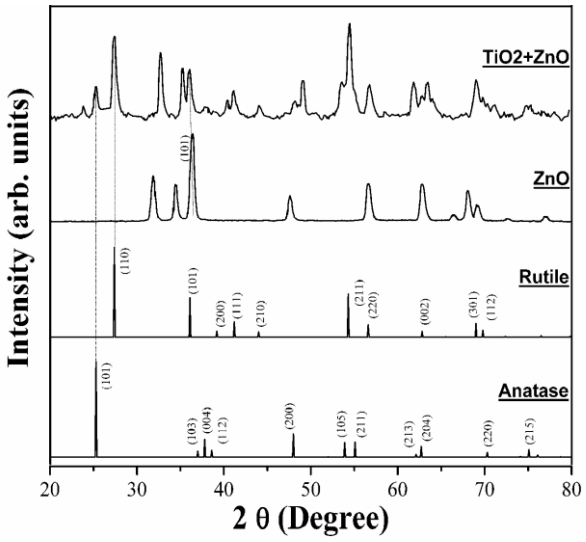

Figure 3. XRD pattern of TiO_2 and ZnO composite

The Scherrer formula calculation for the TiO_2 in the composite produced a crystallite size of 27.71 nm. Remarkably, in composites with Al_2O_3 and WO_3, this size is greater than the crystallite size of TiO_2. Findings revealed that the ZnO crystallite size in the composite is 55.72 nm, a considerable increase above the crystallite sizes of Al_2O_3 and WO_3 in their respective TiO_2 composites. According to XRD studies, the insulator material selection affects the development of mixed oxide systems at the interface between insulator materials and TiO_2. In composite materials, the insulator material selection affects the crystallite size as well.

3.2.4 TiO_2-CNT composite

Figure 4 shows TiO_2's XRD pattern in combination with a carbon nanotube (CNT) insulating material. Whereas the two bottom contours of the third graph show the X-ray diffraction peaks of TiO_2's anatase and rutile phases, the X-ray diffraction of CNT with a crystallite size of 20.4 nm is shown here. The XRD pattern of the as-synthesized TiO_2-CNT composite is illustrate in the upper graph. The XRD pattern of the composite demonstrates a substantial increase in the quantity of anatase TiO_2. Suggesting the formation of the anatase phase, the (211) planes exhibit the maximum intensity peak. The XRD pattern confirms the presence of CNT in the composite by exhibiting a CNT peak at 26°. Additionally, the peak at 63.3° suggests that the sample contains titanium oxide and carbon. It is anticipated that this system will emerge at the interface of CNT and TiO_2, indicating that CNT growth has taken place on the surface of TiO_2.

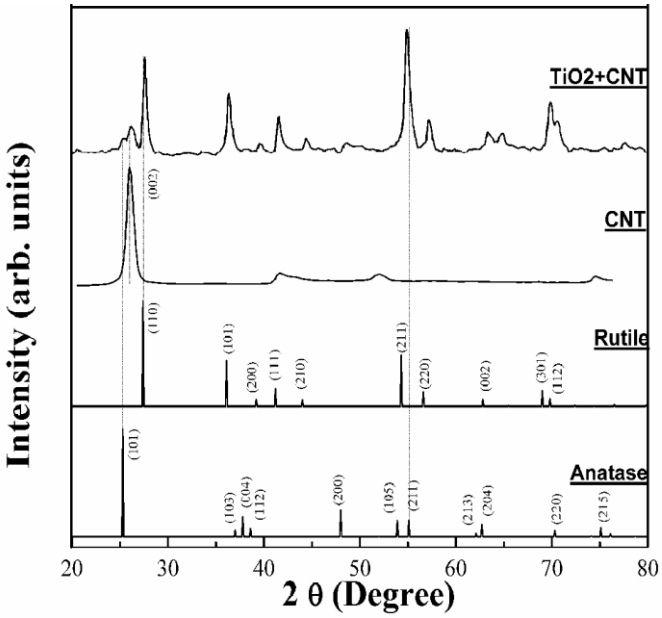

Figure 4. XRD pattern of TiO_2- CNT composite

The crystallite size of TiO_2, which is 26.32 nm, is calculated from its full width at half maximum (FWHM) using the Scherrer formula. The XRD pattern of the TiO_2-CNT composite is crucial for confirming the effective synthesis of the molecule since it provides details on the crystalline phases and sizes present.

3.4.5 TiO_2-SiNT composite

Figure 5 shows the XRD pattern of TiO_2 by use of silicon nanotubes (SiNT), the insulator material. The X-ray diffraction of SiNT is shown in the third graph. The XRD peaks of anatase and rutile phases of TiO_2 are shown in the bottom two graphs. The XRD pattern of TiO_2 that was generated using SiNT is depicted in the upper graph. According to the XRD pattern, the composite has experienced a substantial increase in the quantity of anatase TiO_2. The anatase phase is evident in the peak of maximum intensity for the (101) planes. The XRD pattern's peak at 48.7° provides evidence that SiNT is present in the composite. Peaks at 23° indicate the existence of a silicon-titanium oxide system in the sample. This system most likely developed at the interface between SiNT and TiO_2, indicating that SiNT has grown on TiO_2's surface.

The crystallite size of TiO_2 is determined from the FWHM using the Scherrer formula, which yields 11.15 nm. This value suggests that the composite contains relatively small TiO_2 particles. The XRD pattern of the TiO_2-SiNT composite is essential for determining the crystalline phases and sizes present in the composite, thereby verifying the effective synthesis. SiNT may provide the composite with

supplementary properties, such as enhanced electronic conductivity, which could be advantageous in a variety of industries, including solar energy conversion and photocatalysis.

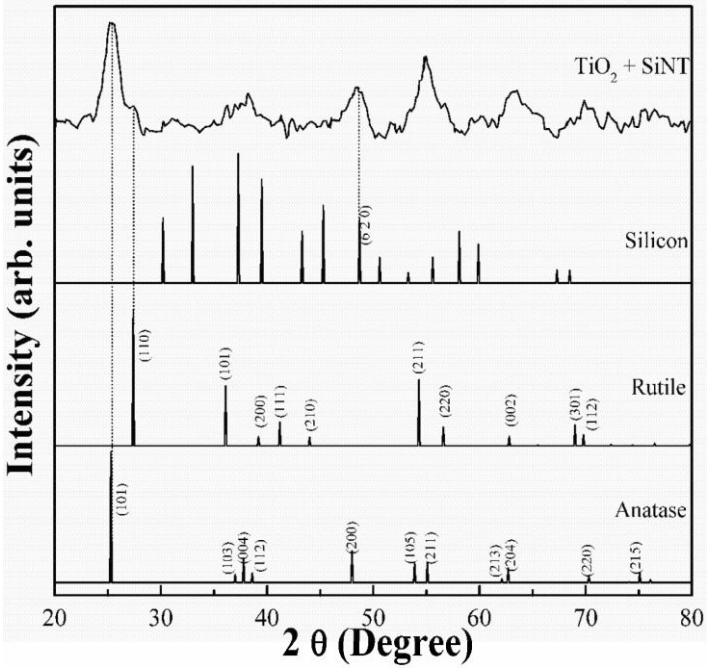

Figure 5. XRD pattern of the TiO_2-SiNT composite

3.2 BET ANALYSIS

Table 1 shows the effective surface area of the composites, calculated using the BET technique from nitrogen adsorption measurements. The samples were tested to establish the specific surface area and average crystallite size. The composite material has a specific surface area of 32.1 m2/gm and average crystallite size of 18.09 nm. TiO_2 + WO_3 has a higher specific surface area (51.4 m2/gm) and a slightly smaller average crystallite size (15.36 nm). The TiO_2 + ZnO combination has the largest and lowest specific surface areas, with an average crystallite size of 27.71 nm and 15.2 m2/gm. The composite material has a specific surface area of 33.2 m2/gm and average crystallite size of 26.32 nm. The combination of TiO_2 + SiNT has the largest specific surface area (93.1 m2/gm) and the shortest average crystallite size (11.15 nm).

The results indicate that including CNT and SiNT in TiO_2 reduces the average crystallite size and increases the specific surface area. The special structure of the nanotubes, marked by their porous character and large surface area, most likely explains this phenomena. Specifically, this structure helps TiO_2 nanoparticles to accumulate. Reducing the average crystallite size of TiO_2 was shown to be equivalent depending on WO_3 and Al_2O_3. Their influence on the particular surface area was really negligible, however. Still, adding ZnO caused an average crystallite size to rise and specific surface area to drop. The larger particle size of ZnO compared to TiO_2 could potentially provide an explanation for this phenomenon. According to BET's investigation, the inclusion of nanotubes, specifically SiNT, in TiO_2 composites has the potential to greatly enhance their specific surface area.

Table 1 Surface area and crystallite size for different TiO_2 Composites.

Sr.	Sample	Avg. Crystallite	Specific Surface
1	TiO_2+Al_2O_3	18.09	32.1
2	TiO_2+WO_3	15.36	51.4
3	TiO_2+ZnO	27.71	15.2
4	TiO_2+CNT	26.32	33.2
5	TiO_2+SiNT	11.15	93.1

Recent research has revealed exciting advancements in enhancing the photocatalytic activity and surface area-based applications of composites, as indicated by several studies [11, 15, 22, 32].

3.3 UV-VISIBLE Composites Analysis

Figure 6 displays the UV-vis absorption spectra of the synthesized TiO_2 composites. The table displays the band gap values of different composites containing TiO_2. In comparison to TiO_2, composites display larger band gaps, indicating reduced photocatalytic activity. When comparing TiO_2 alone to combinations of TiO_2 + Al_2O_3 and TiO_2 + SiNT, it is evident that the latter two exhibit a larger band-gap value. This suggests that they possess higher levels of photocatalytic activity. These substances have

the potential to decrease electron activation, thereby inhibiting photocatalytic processes. This might happen because these materials increase electron-hole pairs and photocatalytic processes [7].

Based on an investigation, scientists have shown that the TiO_2 + WO_3 Composite exhibits the lowest band gap value and the maximum photocatalytic activity [29]. Studying the strong electron affinity of WO_3 can help us understand the occurrence of electron-hole pair generation. As a materials scientist, one can observe a significant enhancement in the photocatalytic activity. Based on the UV analysis findings, the addition of specific materials to TiO_2 can have a significant impact on its photocatalytic activity. Thus, it is crucial to thoroughly assess the characteristics of various materials and how they interact with TiO_2 before drawing any conclusions. The graph displays the band gap values derived from the data in Table 2.

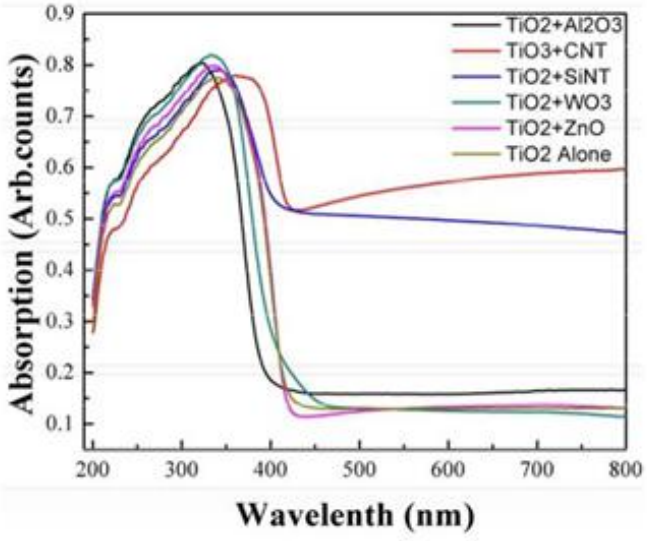

Figure 6. The UV-vis spectra of TiO_2 composites.

Table 2. Band gap values of different composites with TiO_2

TiO_2 Composites	Support Materials	Crystallite Size (nm)	Specific Surface Area (m^2/gm)	Band Gap (eV)
TiO_2	-	15.26	44.08	3.00
TiO_2-Al_2O_3	Al_2O_3	18.09	32.1	3.10
TiO_2-WO_3	WO_3	15.36	51.4	3.01
TiO_2-ZnO	ZnO	27.71	15.2	3.05
TiO_2-CNT	CNT	26.32	33.2	3.03
TiO_2-SiNT	SiNT	11.15	93.1	3.14

Combining titanium dioxide (TiO_2) with other elements helps to produce materials known as TiO_2 compounds that improve their characteristics. They work in fields like photocatalysis and energy storage. Among the many composite support materials included in the data are Al_2O_3, WO_3, ZnO, CNTs, and SiNTs. The features of the material depend much on the range of crystallite sizes (15.26 to 16.7 nm). From 44.08 to 93.1 m2/g, the range of particular surface areas seen in the research is very large. This large spectrum points to the existence of a noteworthy surface area ready for many kinds of responses. Electrical conductivity and light absorption are substantially affected by the range of band gaps, which runs from 3.00 to 3.14 eV. TiO_2 composites have a wide spectrum of characteristics that one may change to fit different uses.

3.4 Photocatalytic Dye Degradation

The photocatalytic degradation of methylene blue (MB) was assessed by monitoring its UV-Visible absorbance at 664 nm. TiO_2 samples calcined at different temperatures were tested under UV light for 30 minutes, with TiO_2 calcined at 550°C showing the highest degradation, as indicated by the steepest drop in absorbance in Figure 7. The absorbance reduced from 1.0 to 0.15, demonstrating enhanced crystallinity, reduced defect states, and increased catalytic sites in the anatase phase.

Further analysis of calcination time at 550°C revealed that TiO_2 calcined for 6 hours exhibited the most effective MB degradation, as shown in Figure 8. The absorbance decreased from 1.0 to 0.08, confirming that this duration optimizes the crystalline phase and surface area without excessive grain growth, ensuring maximum photocatalytic efficiency, as supported by studies on nanocomposite photocatalysts.

The use of TiO_2 composites with support materials such as WO_3 and SiNT further improved photocatalytic performance. Figure 9. illustrates that the TiO_2-WO_3 composite achieved the highest degradation, with absorbance decreasing from 1.0 to 0.05, followed by TiO_2-SiNT at 0.10. This enhancement is due to the lower bandgap of WO_3, which improves visible light absorption and charge transfer.

Photocatalysis in TiO_2 occurs through photon absorption, exciting electrons to the conduction band and generating electron-hole pairs. These pairs initiate redox reactions, forming superoxide ($O_2^{\bullet -}$) and hydroxyl radicals (•OH), which effectively break down MB into non-toxic products. However, charge recombination can reduce efficiency, highlighting the importance of materials that promote charge separation for enhanced photocatalytic applications.

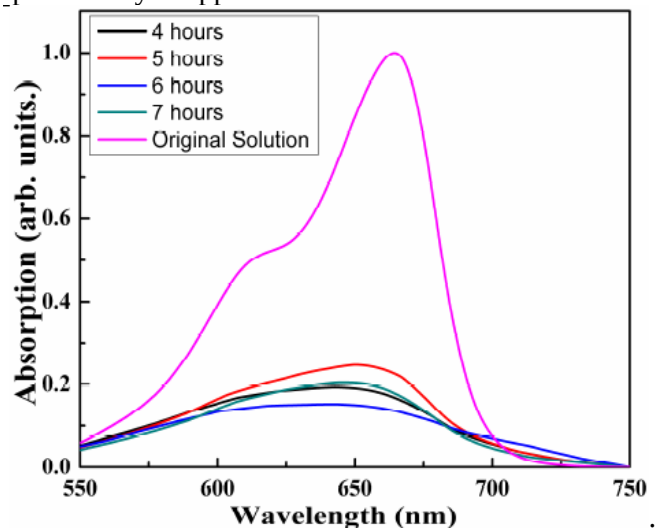

Figure 7. UV-Visible Absorption graph of MB after degradation using as synthesized TiO2 samples calcined for different times

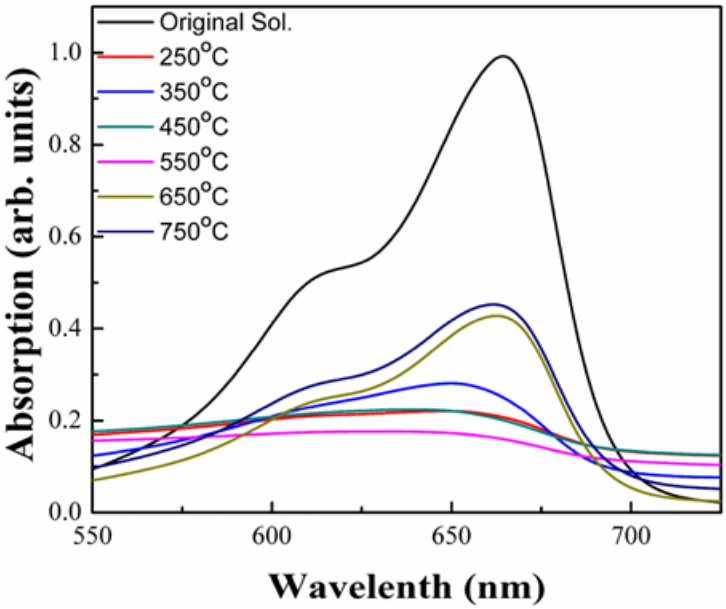

Figure 8. UV-Visible Absorption graph of MB after degradation using as synthesized TiO2 samples calcined at different temperatures

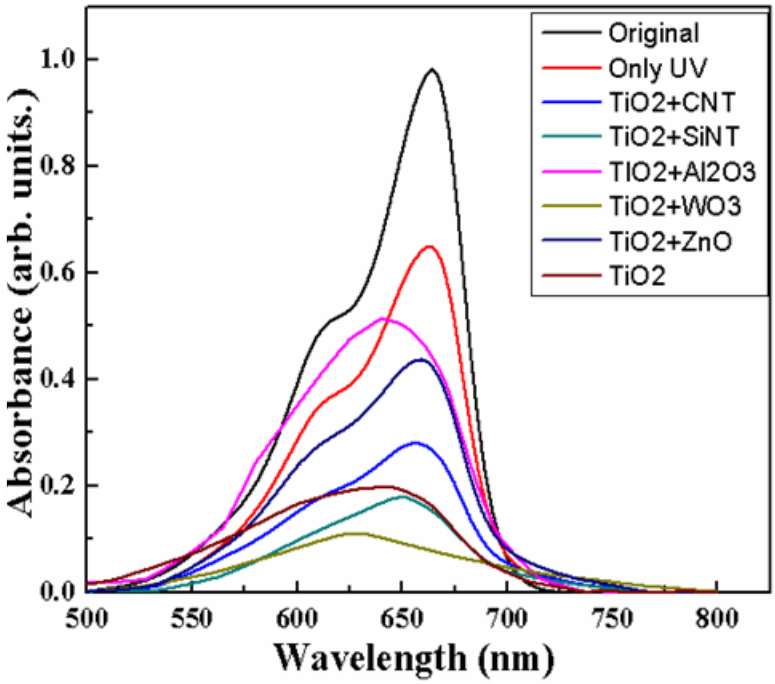

Figure 9. UV-Visible Absorption graph of MB after degradation using as synthesized composites of TiO2

4. Conclusion

In this study, the Sol-Gel technique was successfully employed to evaluate the effects of various additives and optimize the band gap characteristics of TiO_2 composites. Comprehensive investigations confirmed the phase formation, crystal size, and band structure of TiO_2-based compounds, particularly focusing on Al_2O_3, WO_3, ZnO, and SiNT additives. The results revealed that different chemical additions to TiO_2 compounds resulted in diverse crystal structures and lattice parameters, which significantly influenced their properties and potential applications.

After extensive testing, it was found that the ideal calcination temperature for TiO_2 was 550°C for six hours. The formation of mixed oxide systems such as TiO_2-Al_2O_3 and TiO_2-WO_3 composites was confirmed, indicating the presence of separate components on the surface of TiO_2. Variations in crystal size, ranging from 15.26 nm to 18.1 nm, demonstrated the impact of different additives on crystal morphology. Notably, the TiO_2-SiNT composite exhibited a remarkable specific surface area of 93.1 m^2/g, highlighting its potential for high-resolution applications.

The TiO_2 composites displayed varying band gap values, with TiO_2-Al_2O_3, TiO_2-WO_3, TiO_2-ZnO, and TiO_2-SiNT composites showing a band gap of 3.14 eV, compared to the pure TiO_2, which had a band gap of 3.00 eV. These variations in band gap were attributed to the different additives incorporated into the composites. Furthermore, the absorption spectrum analysis revealed significant modifications in the band structure of the TiO_2 composites, opening avenues for new applications in materials science.

In conclusion, this work contributes significantly to the understanding of TiO_2 composites, enhancing our knowledge of their practical applications. Future research should prioritize the practical use and further assessment of these composites, fostering the development of innovative and versatile materials for a wide range of applications.

References

1. Amorim, S. M., Steffen, G., de S Junior, J. M., Brusamarello, C. Z., Romio, A. P., & Domenico, M. D. (2021). Synthesis, characterization, and application of polypyrrole/TiO2 composites in photocatalytic processes: a review. Polymers and Polymer Composites, 29(7), 1055-1074.
2. Anandan, S., & Wu, J. J. (2014). Ultrasound assisted synthesis of TiO2–WO3 heterostructures for the catalytic degradation of Tergitol (NP-9) in water. Ultrasonics sonochemistry, 21(4), 1284-1288.
3. Bazli, L., Siavashi, M., & Shiravi, A. (2019). A review of carbon nanotube/TiO2 composite prepared via sol-gel method. Journal of Composites and Compounds, 1(1), 1-9.

4. Garzon-Roman, A., Quiroga-Gonzalez, E., & Zuniga-Islas, C. (2021). Heterostructure of TiO2 and macroporous silicon: The simplest relaxation oscillator. Journal of Science: Advanced Materials and Devices, 6(2), 209-214..
5. Balasamy, R. J., Khurshid, A., Al-Ali, A. A., Atanda, L. A., Sagata, K., Asamoto, M., ... & Al-Khattaf, S. S. (2010). Ethylbenzene dehydrogenation over binary FeOx–MeOy/Mg (Al) O catalysts derived from hydrotalcites. Applied Catalysis A: General, 390(1-2), 225-234..
6. Gupta, S. M., & Tripathi, M. (2011). A review of TiO 2 nanoparticles. chinese science bulletin, 56, 1639-1657.
7. Hastuti, L. P., Kusumaatmaja, A., Darmawan, A., & Kartini, I. (2022). Effect of polymer concentration on the photocatalytic membrane performance of PAN/TiO2/CNT nanofiber for methylene blue removal through cross-flow membrane reactor. Bulletin of Chemical Reaction Engineering & Catalysis, 17(2), 350-362.
8. He, J., Kumar, A., Khan, M., & Lo, I. M. (2021). Critical review of photocatalytic disinfection of bacteria: from noble metals-and carbon nanomaterials-TiO2 composites to challenges of water characteristics and strategic solutions. Science of the Total Environment, 758, 143953.
9. Hemalatha, K., Ette, P. M., Madras, G., & Ramesha, K. (2015). Visible light assisted photocatalytic degradation of organic dyes on TiO 2–CNT nanocomposites. Journal of Sol-Gel Science and Technology, 73, 72-82.
10. Iliev, V., Tomova, D., Rakovsky, S., Eliyas, A., & Puma, G. L. (2010). Enhancement of photocatalytic oxidation of oxalic acid by gold modified WO3/TiO2 photocatalysts under UV and visible light irradiation. Journal of Molecular Catalysis A: Chemical, 327(1-2), 51-57.
11. Jeon, B. J., & Lee, J. K. (2011). Electrochemical characteristics of porous TiO2 encapsulated silicon anode. Electrochimica acta, 56(18), 6261-6265.
12. Jian, H., Du, Q., Men, Q., Guan, L., Li, R., Fan, B., ... & Zhang, R. (2022). Structure-dependent electromagnetic wave absorbing properties of bowl-like and honeycomb TiO2/CNT composites. Journal of Materials Science & Technology, 109, 105-113.
13. [13] Prashanth, M., Karunanithi, R., Mohideen, S. R., Sivasankaran, S., & Vlahović, M. (2023). A comparative study on X-ray peak broadening analysis of mechanically alloyed Al2O3 particles dispersion strengthened Al 7017 alloy. Materials Chemistry and Physics, 294, 127015.
14. Kaseem, M., Hamad, K., & Ur Rehman, Z. (2019). Review of recent advances in polylactic acid/TiO2 composites. Materials, 12(22), 3659.
15. de la Flor, M. P., Camarillo, R., Martínez, F., Jiménez, C., Quiles, R., & Rincon, J. (2022). Synthesis and characterization of bimetallic TiO2/CNT/Pd-Cu for efficient remediation of endocrine disruptors under solar light. Journal of Environmental Chemical Engineering, 10(2), 107245.
16. de la Flor, M. P., Camarillo, R., Martínez, F., Jiménez, C., Quiles, R., & Rincón, J. (2021). Synthesis and characterization of TiO2/CNT/Pd: An effective sunlight photocatalyst for neonicotinoids degradation. Journal of Environmental Chemical Engineering, 9(5), 106278.
17. Yu, S. H., Kang, Y., & Lee, C. G. (2023). Comparison of the spray effects of air induction nozzles and flat fan nozzles installed on agricultural drones. Applied Sciences, 13(20), 11552.
18. Li, R., Li, T., & Zhou, Q. (2020). Impact of titanium dioxide (TiO2) modification on its application to pollution treatment—a review. Catalysts, 10(7), 804..
19. Salomón-Flores, M. K., Hernández-Juárez, C. L., Bazany-Rodríguez, I. J., Barroso-Flores, J., Martínez-Otero, D., López-Arteaga, R., ... & Dorazco-González, A. (2019). Efficient fluorescent chemosensing of iodide based on a cationic meso-tetraarylporphyrin in pure water. Sensors and Actuators B: Chemical, 281, 462-470.
20. Simon, S. M., George, G., Sajna, M. S., Prakashan, V. P., Jose, T. A., Vasudevan, P., ... & Unnikrishnan, N. V. (2021). Recent advancements in multifunctional applications of sol-gel derived polymer incorporated TiO2-ZrO2 composite coatings: A comprehensive review. Applied Surface Science Advances, 6, 100173.
21. Miyake, M., Takahashi, A., & Hirato, T. (2017). Electrodeposition and anodization of Al-TiO2 composite coatings for enhanced photocatalytic activity. International Journal of Electrochemical Science, 12(3), 2344-2352.
22. Moradi, S., Aberoomand-Azar, P., Raeis-Farshid, S., Abedini-Khorrami, S., & Givianrad, M. H. (2016). The effect of different molar ratios of ZnO on characterization and photocatalytic activity of TiO2/ZnO nanocomposite. Journal of Saudi Chemical Society, 20(4), 373-378.
23. Muscetta, M., Andreozzi, R., Clarizia, L., Di Somma, I., & Marotta, R. (2020). Hydrogen production through photoreforming processes over Cu2O/TiO2 composite materials: A mini-review. International Journal of Hydrogen Energy, 45(53), 28531-28552. Reghunath, S., Pinheiro, D., & KR, S. D. (2021). A review of hierarchical nanostructures of TiO2: Advances and applications. Applied Surface Science Advances, 3, 100063.
24. Rehman, Z. U., Bilal, M., Hou, J., Butt, F. K., Ahmad, J., Ali, S., & Hussain, A. (2022). Photocatalytic CO2 reduction using TiO2-based photocatalysts and TiO2 Z-scheme heterojunction composites: a review. Molecules, 27(7), 2069.

25. Rosales, A., & Esquivel, K. (2020). SiO2@ TiO2 composite synthesis and its hydrophobic applications: A review. Catalysts, 10(2), 171.
26. Sampath, S., Maydannik, P., Ivanova, T., Shestakova, M., Homola, T., Bryukvin, A., ... & Alagan, V. (2016). Efficient solar photocatalytic activity of TiO2 coated nano-porous silicon by atomic layer deposition. Superlattices and Microstructures, 97, 155-166.
27. Shifu, C., Lei, C., Shen, G., & Gengyu, C. (2005). The preparation of coupled WO3/TiO2 photocatalyst by ball milling. Powder technology, 160(3), 198-202.
28. Shon, H. K., Phuntsho, S., Vigneswaran, S., Kandasamy, J., Nghiem, L. D., Kim, G. J., ... & Kim, J. H. (2010). Preparation of titanium dioxide nanoparticles from electrocoagulated sludge using sacrificial titanium electrodes. Environmental science & technology, 44(14), 5553-5557.
29. Someswararao, M. V., Dubey, R. S., & Subbarao, P. S. V. (2021). Electrospun composite nanofibers prepared by varying concentrations of TiO2/ZnO solutions for photocatalytic applications. J. Photochem. Photobiol, 6(10001610.1016).
30. Tian, X., Cui, X., Lai, T., Ren, J., Yang, Z., Xiao, M., ... & Wang, Y. (2021). Gas sensors based on TiO2 nanostructured materials for the detection of hazardous gases: A review. Nano Materials Science, 3(4), 390-403.
31. Tsukamoto, D., Ikeda, M., Shiraishi, Y., Hara, T., Ichikuni, N., Tanaka, S., & Hirai, T. (2011). Selective photocatalytic oxidation of alcohols to aldehydes in water by TiO2 partially coated with WO3. Chemistry–A European Journal, 17(35), 9816-9824.
32. Wang, C. C., Wang, X., & Liu, W. (2020). The synthesis strategies and photocatalytic performances of TiO2/MOFs composites: a state-of-the-art review. Chemical Engineering Journal, 391, 123601.
33. Yuan, X., Ye, Y., Lian, M., & Wei, Q. (2018). Structural coloration of polyester fabrics coated with Al/TiO2 composite films and their anti-ultraviolet properties. Materials, 11(6), 1011.
34. Shikika, A., Sethurajan, M., Muvundja, F., & Mugumaoderha, M. C. (2020). A review on extractive metallurgy of tantalum and niobium. Hydrometallurgy, 198, 105496.
35. Al Zoubi, W., Al-Hamdani, A.A.S., Sunghun, B., & Ko, Y.G. (2021). A review on TiO_2-based composites for superior photocatalytic activity. Reviews in Inorganic Chemistry, 41(3), 213–238